A robust causality verification tool for tabulated frequency data

P. Triverio, S. Grivet-Talocia
Dept. of Electronics, Politecnico di Torino
C. Duca degli Abruzzi 24, 10129 Torino, Italy
Email: piero.triverio@polito.it, grivet@polito.it

Abstract

We introduce a robust algorithm for the qualification of tabulated frequency data representing the port responses of a linear subsystem. This algorithm is aimed at the verification that frequency responses obtained via full-wave electromagnetic simulation or from direct measurement of some interconnect structure are self-consistent and causal before they are used for the generation of macromodels for system-level analysis and design purposes. The technique is based on an advanced formulation of the Hilbert transform, leading to a direct check for causality of the raw data. One of the main advantages of the proposed method is the possibility to provide accurate estimates for error bounds due to various sources, including sampling frequency and data availability over a limited bandwidth.

Introduction and motivations

The design of high-speed interconnect structures is usually based on systematic simulation at component, subsystem, and system level. These simulations are based on suitable models for the various subparts of the system, which must represent all relevant electromagnetic phenomena that have some influence both on signal and power/ground quality. Considering one of these substructures (e.g., a connector or a via array), the first step for the derivation of such a model is to perform some full-wave electromagnetic simulation of the structure, in order to obtain a set of port responses in the form of frequency tables for the scattering, impedance, or admittance matrix. Alternatively, these port responses can be obtained from direct measurement if the hardware is available.

When frequency responses are available, several techniques (e.g., the very popular Vector Fitting (VF) algorithm [1]) can be used for the derivation of macromodels that can be used for transient simulation in standard circuit-based solvers. However, a good model can only be derived from good data. The raw frequency responses may be affected by noise in case of direct measurement, or by frequency-dependent numerical errors when coming from full-wave simulations. Also, such data are naturally available over a limited frequency range and with a limited number of discrete frequency samples. All these facts may lead to failure of the macromodeling algorithm, which can in some cases fail to converge or lead to inaccurate results. It is often difficult to discriminate whether these difficulties are due to flaws and inconsistencies in the raw frequency responses or to a poor performance/misuse of the macromodeling algorithm.

We propose in this paper a technique for the verification of causality of raw frequency data. It is well-known that real and imaginary parts of any frequency response representing a causal system are related by Hilbert transform. Direct verification of causality via Hilbert transform, however, is numerically difficult. We propose an advanced formulation of the Hilbert transform based on a regularization procedure, which allows to verify the causality without numerical difficulties. In addition, error bounds in this verification process due to finite sampling frequency and bandwidth are explicitly computed and used to unbias the causality check from systematic errors. Several test cases are considered to illustrate that causality violations are quite common in practical situations. We show that when no countermeasures are taken, serious inconsistencies may arise in the macromodel generation and its further use for system-level analysis and design.

Causality and Hilbert transform

We consider a linear interconnect structure with input-output behavior described by

$$\mathbf{y}(t) = \mathbf{h}(t) * \mathbf{x}(t) \quad \Leftrightarrow \quad \mathbf{Y}(j\omega) = \mathbf{H}(j\omega)\mathbf{X}(j\omega)\,, \qquad (1)$$

with $\mathbf{x}(t)$ collecting the electrical variables assumed as inputs, $\mathbf{y}(t)$ the outputs, and $\mathbf{h}(t)$ being the system impulse response matrix. The corresponding frequency-domain representation involves the system transfer matrix $\mathbf{H}(j\omega)$, typically the impedance, admittance or scattering matrix according to the adopted representation. Throughout this work we will present results that apply to any entry of the transfer matrix. Therefore, without loss of generality, we will consider a generic scalar transfer function $H(j\omega) = U(\omega) + jV(\omega)$, with U and V denoting its real and imaginary parts as functions of frequency.

Causality is a basic principle stating that any effect must not precede its cause. This causality principle requires the system impulse response to be vanishing for negative times, $h(t) = 0, \ t < 0$. This condition, when expressed in frequency domain, implies that the real and imaginary parts of the transfer matrix are not independent but are related by Hilbert transform or, equivalently, satisfy the Kramers-Krönig dispersion relations

$$U(\omega) = \frac{1}{\pi} \fint V(\omega') \frac{d\omega'}{\omega - \omega'} \qquad (2a)$$

$$V(\omega) = -\frac{1}{\pi} \fint U(\omega') \frac{d\omega'}{\omega - \omega'} \qquad (2b)$$

where all integrals are defined according to Cauchy principal value. Throughout this paper, unless explicitly noted, any integral extends from $-\infty$ to $+\infty$. The following theorem [2, 3] summarizes the three basic conditions (with some technical restrictions, not given here) that characterize a causal system

Theorem 1. *The following facts are equivalent:*

(i) $h(t) = 0$ *for* $t < 0$*;*

(ii) the dispersion relations (2a)-(2b) hold;

(iii) $H(j\omega)$ *is the limit as* $\sigma \to 0$ *of a function* $H(s) = H(\sigma + j\omega)$ *analytic and of polynomial growth for* $\sigma > 0$*.*

Robust causality check with error bounds

We assume that the following discrete set of samples

$$H(j\omega_k), \quad k = 1, \ldots, K \tag{3}$$

is known, with $\omega_1 = 0$ and $\omega_K = B$ defining the bandwidth over which raw frequency responses are available. Due to the symmetry of the spectrum of real signals, we can assume data available also for negative frequencies. The main objective of this paper is to provide a robust verification for the consistency of the available data points (3) with the dispersion relations (2a)-(2b). This involves the reconstruction of the real (imaginary) part of the data starting form the imaginary (real) one using some discretized form of (2a)-(2b). If we denote the reconstructed transfer function as $\widehat{H}(j\omega)$, a frequency-dependent consistency error may be defined as

$$\Delta(j\omega_k) = |\widehat{H}(j\omega_k) - H(j\omega_k)|, \quad k = 1, \ldots, K \tag{4}$$

A causality violation will be detected when this error results larger than some suitable threshold. The precise definition of this threshold is one of the main results of this paper and is given in the following.

The direct discretization of (2a)-(2b) fails due to the following reasons

- Raw data are available up to a maximum frequency B, whereas Hilbert transform must be defined by integration over the entire frequency axis from $-\infty$ to $+\infty$. This leads to an unavoidable truncation error in the numerical evaluation of dispersion relations. This error source may be very critical since $H(j\omega)$ may not decay to zero for large frequencies (it may even grow for $\omega \to \infty$ in the case of impedance or admittance representations). This implies that the contribution of $|\omega| > B$ to the integral may not be negligible and must be dealt with in some way.
- Only a discrete number of frequency samples is available. This introduces a discretization error in the numerical evaluation of the dispersion relations, which is dependent on the sampling interval. This error is magnified by the singular nature of the Hilbert kernel $(\omega - \omega')^{-1}$. An accurate numerical evaluation calls for some regularization procedure to account for this singularity.

These two facts contribute to numerical errors in the evaluation of the dispersion integrals, which may be so large to hide even quite significant causality violations. Therefore, we propose an alternative formulation of the Hilbert transform pair, that guarantees an effective handling of the above difficulties and allows an accurate estimate of the resulting numerical errors. In turn, these estimates provide a rigorous frequency-dependent threshold to compare the reconstruction error (4) with.

Generalized dispersion relations with subtractions. Instead of (2a)-(2b), we suggest to use the so-called dispersion relations with subtractions [4], defined as

$$U(\omega) = \alpha_U(\omega) + \frac{\omega^n}{\pi} \fint \frac{V(\omega') - \alpha_V(\omega')}{(\omega')^n} \frac{d\omega'}{\omega - \omega'} \tag{5a}$$

$$V(\omega) = \alpha_V(\omega) - \frac{\omega^n}{\pi} \fint \frac{U(\omega') - \alpha_U(\omega')}{(\omega')^n} \frac{d\omega'}{\omega - \omega'} \tag{5b}$$

where

$$\alpha_U(\omega) = \sum_{\nu=0}^{n-1} \frac{U^{(\nu)}(0)}{\nu!}\omega^\nu \quad \alpha_V(\omega) = \sum_{\nu=0}^{n-1} \frac{V^{(\nu)}(0)}{\nu!}\omega^\nu$$

and n is the number of subtractions. These expressions are readily obtained by subtracting the n-th order Taylor polynomial from $H(j\omega)$, dividing the result by ω^n, and finally applying the standard Hilbert transform. It can be shown that if $H(j\omega)$ satisfies (5a) and (5b), the system is causal, i.e., these two generalized dispersion relations are fully equivalent to (2a)-(2b). The two main advantages of this formulation are: (i) applicability for arbitrary $H(j\omega)$, including the case of no asymptotic decay; (ii) reduced sensitivity to the high-frequency behavior of $H(j\omega)$. Unfortunately, their numerical evaluation requires the estimation of the n-th order Taylor polynomial, which becomes ill-conditioned in case of discrete data as in (3), since numerical evaluation of high-order derivatives is implied.

We overcome this last difficulty as follows. High-order derivatives are needed to compensate the strong singularity in $\omega = 0$ arising from the division by the polynomial ω^n. However, we can distribute the roots of this polynomial at different frequencies $\bar{\omega}_q$ instead of in $\omega = 0$. We obtain

$$\begin{aligned} U(\omega) &= \beta_U(\omega) + \frac{\prod_{q=1}^n(\omega - \bar{\omega}_q)}{\pi} \fint \frac{V(\omega') - \beta_V(\omega')}{\prod_{q=1}^n(\omega' - \bar{\omega}_q)} \frac{d\omega'}{\omega - \omega'} \\ V(\omega) &= \beta_V(\omega) - \frac{\prod_{q=1}^n(\omega - \bar{\omega}_q)}{\pi} \fint \frac{U(\omega') - \beta_U(\omega')}{\prod_{q=1}^n(\omega' - \bar{\omega}_q)} \frac{d\omega'}{\omega - \omega'} \end{aligned} \tag{6}$$

where $\beta_F(\omega) = \sum_{q=1}^n l_q(\omega) F(\bar{\omega}_q)$ for $F = \{U, V\}$ and

$$l_q(\omega) = \prod_{\substack{p=1 \\ p \neq q}}^{n} \frac{\omega - \bar{\omega}_p}{\bar{\omega}_q - \bar{\omega}_p} \text{ (Lagrange interpolation polynomials)}$$

These relations make only use of function evaluation at the subtraction points $\bar{\omega}_q$, leading to use of the more stable Lagrange polynomials. Optimal placement of the subtraction points is discussed below.

Truncation error: estimation and accuracy optimization. For the sake of brevity we focus on the first line in (6), but the following developments apply to both dispersion relations. The truncation error is due to data availability in a finite bandwidth $[-B, B]$ and equals, for $|\omega| < B$,

$$\tilde{E}_n(\omega) = \frac{\prod_{q=1}^n(\omega - \bar{\omega}_q)}{\pi} \int_{\Omega_B} \frac{V(\omega') - \beta_V(\omega')}{\prod_{q=1}^n(\omega' - \bar{\omega}_q)} \frac{d\omega'}{\omega - \omega'} \tag{7}$$

where Ω_B identifies the frequencies outside $[-B, B]$. This error can be split into two separate contributions

$$\begin{aligned} \tilde{E}_n(\omega) = &\underbrace{\frac{\prod_{q=1}^n(\omega - \bar{\omega}_q)}{\pi} \int_{\Omega_B} \frac{V(\omega')}{\prod_{q=1}^n(\omega' - \bar{\omega}_q)} \frac{d\omega'}{\omega - \omega'}}_{E_n(\omega)} + \\ &\underbrace{- \frac{\prod_{q=1}^n(\omega - \bar{\omega}_q)}{\pi} \int_{\Omega_B} \frac{\beta_V(\omega')}{\prod_{q=1}^n(\omega' - \bar{\omega}_q)} \frac{d\omega'}{\omega - \omega'}}_{C(\omega)} \end{aligned} \tag{8}$$

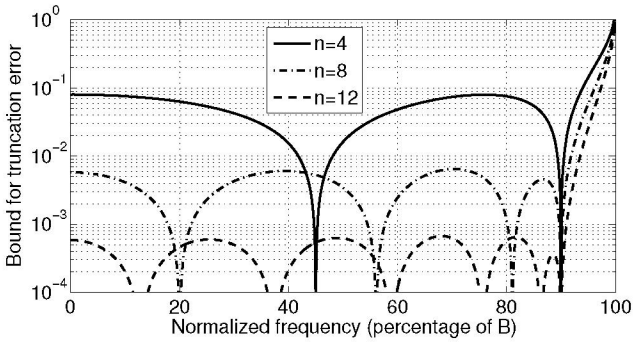

Figure 1: Bound on truncation error as a function of number of subtraction points n with Chebyshev distribution over 90% of the bandwidth B.

The second term $C(\omega)$ can be quite large, but it can be evaluated analitically and corrected. Thus, the truncation error reduces to $E_n(\omega)$ only. A bound for this error term is obtained by assuming a worst-case high-frequency behavior for $H(j\omega)$. This behavior depends on the adopted representation. We derive here such a bound assuming data in scattering form, therefore assuming $|H(j\omega)| \leq 1$ at any frequency. Bounds for other representations such as impedance or admittance can be derived similarly. In the scattering case we obtain the error bound in closed form as

$$|E_n(\omega)| \leq \frac{\prod_{q=1}^{n} |\omega - \bar{\omega}_q|}{\pi} \int_{\Omega_B} \frac{1}{\prod_{q=1}^{n} |\omega' - \bar{\omega}_q|} \frac{d\omega'}{|\omega - \omega'|} =$$

$$T_n(\omega) = \frac{1}{\pi} \sum_{q=1}^{n} \left[\left| \ln \frac{B - \bar{\omega}_q}{B - \omega} \right| - (-1)^n \left| \ln \frac{B + \bar{\omega}_q}{B + \omega} \right| \right] \times$$

$$\times \prod_{\substack{p=1 \\ p \neq q}}^{n} \frac{|\omega - \bar{\omega}_p|}{\bar{\omega}_q - \bar{\omega}_p} \qquad (9)$$

It can be shown that $T_n(\omega)$ remains bounded between any pair of subtraction points. Also, this error can be made arbitrary small by increasing the number of subtractions n. An example is provided in Fig. 1. This important result enables direct accuracy-controlled causality check even for bandlimited data.

The truncation error $T_n(\omega)$ can be further minimized with an appropriate placement of subtraction points $\bar{\omega}_q$. We have verified that a Chebyshev distribution

$$\bar{\omega}_q = -B(1-\epsilon)\cos\frac{(q-1)\pi}{n-1}, \quad q = 1, \ldots, n \qquad (10)$$

guarantees a quasi-optimal truncation error in a bandwidth arbitrarily close ($\epsilon \ll 1$) to $[-B, B]$. The truncation error always diverges near $\omega = \pm B$ due to the intrinsic (two-sided) nature of the Hilbert transform kernel.

Discretization error and singularity extraction. The computation of integrals with principal value in (6) needs special care because integrands are singular for $\omega' = \omega$; a simple but effective approach consists of extracting the singular term

$$\fint_{-B}^{B} g(\omega') \frac{d\omega'}{\omega - \omega'} = \int_{-B}^{B} \frac{g(\omega') - g(\omega)}{\omega - \omega'} d\omega' - g(\omega) \ln \left| \frac{B - \omega}{B + \omega} \right|$$

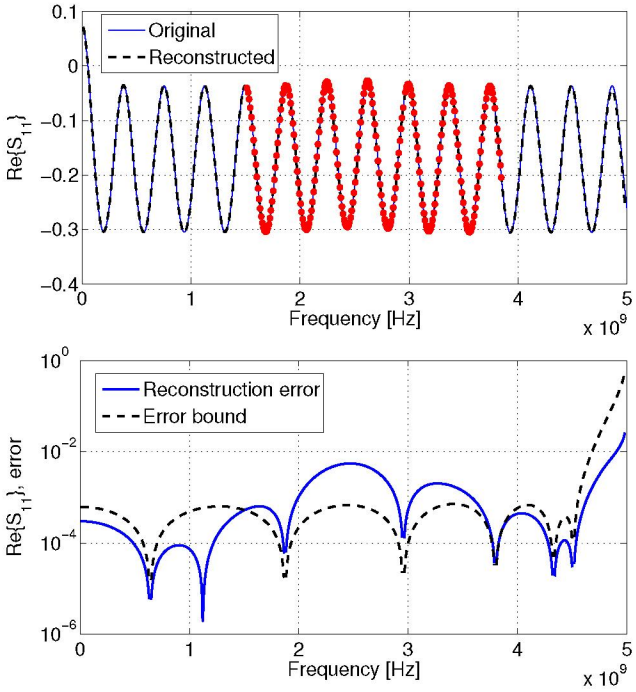

Figure 2: Top panel: Hilbert-reconstructed real part compared to the raw data. Dots denote samples where causality violations are detected. Bottom panel: reconstruction error $\Delta(j\omega)$ compared to the frequency-dependent threshold $E_n^{\text{tot}}(\omega)$.

and computing the remaining non-singular integral with a conventional quadrature algorithm. One can choose the integration method that guarantees the best accuracy/efficiency for the data under examination and possibly provides an estimation of the numerical error $D(\omega)$ affecting the result. In this work, we compute $D(\omega)$ by comparing the results of two different quadrature methods of different order (namely, trapezoidal and Simpson rules).

The causality check. Having identified the various sources of errors, we construct a worst-case frequency-dependent numerical error as

$$E_n^{\text{tot}}(\omega) = T_n(\omega) + D(\omega)\,. \qquad (11)$$

This provides the "resolution" of the numerical tool we have constructed for detecting causality violations. Therefore, the causality check we adopt is

$$\Delta(j\omega_k) \leq E_n^{\text{tot}}(\omega_k), \quad \forall k : |\omega_k| < B(1-\epsilon) \qquad (12)$$

If the above condition is satisfied, any causality violation in the data is not discernible from the numerical errors intrinsic in the Hilbert transform tool. Conversely, if this condition is violated at some frequencies, we are confident that the raw data are not causal, since the accuracy of the numerical tool we use for the check is finer than the violation itself.

Examples

The first example we show is specifically designed to illustrate the excellent resolution of the proposed causality check tool. We consider a uniform transmission line segment with per-unit-length parameters $L = 4.73\,\text{nH/cm}$, $C = 3.8\,\text{pF/cm}$,

$R = 0.8\,\Omega/\mathrm{cm}$, $G = 0$, and length $\mathcal{L} = 10\,\mathrm{cm}$. We computed the scattering matrix of the structure up to 5 GHz. Then, a smooth gaussian-shaped perturbation was added to the real part of $S_{11}(j\omega)$, thus forcing an artificial causality violation. The peak amplitude of the perturbation is 0.01, with an approximate bandwidth of 0.5 GHz, centered around 2.5 GHz. The proposed causality check was applied, by setting a number of subtractions $n = 12$, such that the expected truncation error bound results less than 10^{-3}. Top panel in Fig. 2 shows the excellent accuracy of the proposed Hilbert transform numerical evaluation tool by comparing the perturbed real part to the reconstructed one from the imaginary part. Note that with this scale the causality violation is hardly visible. Bottom panel in Fig. 2 compares the reconstruction error $\Delta(j\omega)$ to the frequency-dependent threshold $E_n^{\mathrm{tot}}(\omega)$. This plot confirms the high resolution of the causality check, which is able in this case to detect even such a small causality violation.

The second example we investigate comes from direct VNA measurements of a long interconnect link (courtesy of IBM). We were actually aware of some flaws in the data before developing and applying the causality verification tool, since we experienced difficulties in trying to identify a macromodel from the data. In fact, application of VF for producing a rational approximation of the scattering matrix entries was not converging and was consistently producing poles with positive real part. A run of the causality check with $n = 6$ subtraction points leads to the results depicted in the top panel of Fig. 3. The presence of causality violations is evident from the portions of the raw data falling outside the allowed frequency-dependent interval obtained by the error bound estimates. Bottom panel in Fig. 3 reports the approximation error obtained by VF as a function of the number of poles used in the approximation. The original dataset shows error stagnation, as a visible symptom of the causality violations. We then used our Hilbert-transform tool to attempt a correction of these causality violations, by replacing the flawed responses with the Hilbert-reconstructed ones. Application of VF to this new "causality-corrected" responses leads to better error convergence. The theoretical background for this behavior is provided by Theorem 1, which states that a non-causal frequency response cannot be analytic in the right-hand complex plane. This is the reason for the consistent emergence of unstable poles during the approximation. More details on these aspects will be documented in a future report.

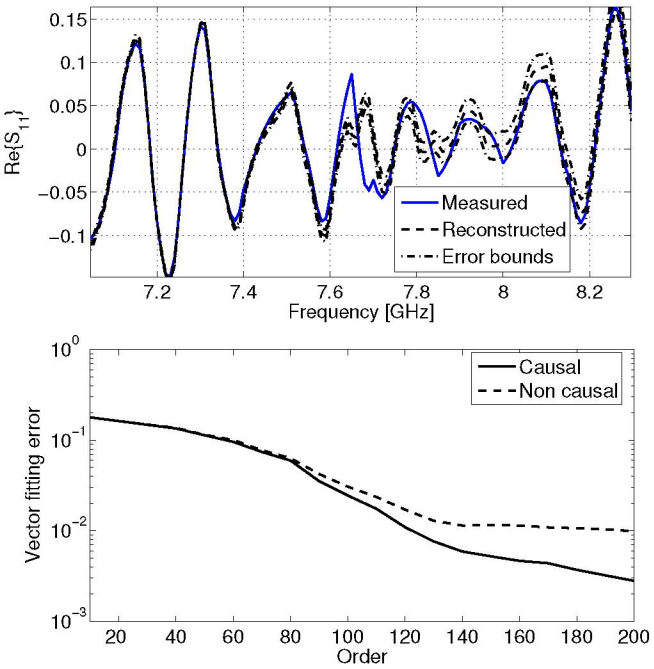

Figure 3: Top panel: Hilbert-reconstructed real part with superimposed error bounds compared to the raw measured data. Bottom panel: evolution of VF approximation error as function of the number of poles for the original non-causal measured data and for the corrected data with enforced causality.

Conclusions

We have presented an advanced numerical technique for detecting causality violations in tabulated frequency responses. The method employs an advanced formulation of the Hilbert transform pair based on a polynomial extraction and a regularization process. The main advantage of this formulation is the availability of error bound estimates in case of application to bandlimited and sampled frequency responses. This is indeed the practical situation when a rigorous check for causality and consistency is needed before proceeding in using the data, e.g. for the generation of a rational macromodel to be employed for analysis and design purposes. The proposed numerical technique is intended to provide a robust validation tool for the automatic qualification of measured/simulated frequency responses. As a final remark, we note that the proposed technique can be readily extended to more restrictive causality definitions accounting for propagation delay effects, e.g., for distributed interconnects and transmission line structures. This extension will be documented in a future report.

Acknowledgments

The Authors are grateful to E. Klink, D. Kaller, and C. Schuster (IBM) for providing the measured data that we used in one of the numerical examples.

References

[1] B. Gustavsen and A. Semlyen, "Rational approximation of frequency domain responses by Vector Fitting," *IEEE Trans. on Power Delivery*, vol. 14, no. 3, pp. 1052–1061, July 1999.

[2] E. C. Titchmarsh, *Introduction to the theory of Fourier integrals*, 2nd ed. Oxford university press, 1948.

[3] E. J. Beltrami, "Linear Dissipative Systems, Nonnegative Definite Distributionals Kernels, and the Boundary Values of Bounder-Real and Positive-Real Matrices," *Journal of Mathematical Analysis and Applications*, vol. 19, pp. 231–246, 1967.

[4] N. M. Nussenzveig, *Causality and dispersion relations*. Academic Press, 1972.